

**SPIN COATING GROWTH AND  
CHARACTERIZATION OF INDIUM NITRIDE  
THIN FILMS**

**LEE ZHI YIN**

**UNIVERSITI SAINS MALAYSIA  
2018**

**SPIN COATING GROWTH AND  
CHARACTERIZATION OF INDIUM NITRIDE  
THIN FILMS**

by

**LEE ZHI YIN**

**Dissertation submitted in fulfillment of the requirements  
for the degree of  
Doctor of Philosophy**

**August 2018**

## ACKNOWLEDGEMENT

First and foremost, I would like to express my deepest gratitude to my supervisor, Assoc. Prof. Dr. Ng Sha Shiong, for his enlightening guidance, encouragement, and patience throughout the course of this research. He has always given me freedom to explore on my own, at the same time providing constant support in the development of this project. Besides, I have been amazingly fortunate to have Assoc. Prof. Dr. Yam Fong Kwong and Prof. Dr. Zainuriah Hassan as my co-supervisors, who accepted me to work in their research facilities, responded to my queries promptly and gave invaluable suggestions during my studies.

Next, I wish to acknowledge the staff at the School of Physics, and the Institute of Nano Optoelectronic Research and Technology (INOR), Universiti Sains Malaysia for their kind assistance in handling the characterization systems. I am also grateful to the members of Dr. Ng's research group for their inspiring discussion and wonderful spirit of sharing knowledge. We are completely different; some of us need a quiet environment to do work, while some need music to get in the mood, and yet we work happily together every day. The most important is that we all share one goal. It has been a great pleasure working and learning with them.

I am thankful for the financial support from the Ministry of Higher Education of Malaysia (MOHE) through the Fundamental Research Grant Scheme (Account No. 203/CINOR/6711453) and MyBrain15 scholarship.

The last but not least, to my dearest friends, thank you for standing by my side, listening and offering me advice all these years. Finally, I am most indebted to

my family for their unconditional love and understanding. Their encouragement gave me confidence to keep moving towards my goal and made me the person I always wanted to be.

## TABLE OF CONTENTS

|  |       |
|--|-------|
| <b>ACKNOWLEDGEMENT</b> .....                   | ii    |
| <b>TABLE OF CONTENTS</b> .....                 | iv    |
| <b>LIST OF TABLES</b> .....                    | ix    |
| <b>LIST OF FIGURES</b> .....                   | x     |
| <b>LIST OF SYMBOLS</b> .....                   | xv    |
| <b>LIST OF ABBREVIATIONS</b> .....             | xviii |
| <b>ABSTRAK</b> .....                           | xx    |
| <b>ABSTRACT</b> .....                          | xxii  |
| <br>   |       |
| <b>CHAPTER 1 – INTRODUCTION</b>                |       |
| 1.1 Introduction .....                         | 1     |
| 1.2 Motivation and problem statements .....    | 4     |
| 1.3 Research objectives .....                  | 5     |
| 1.4 Originality .....                          | 6     |
| 1.5 Dissertation organization .....            | 7     |
| <br>   |       |
| <b>CHAPTER 2 – LITERATURE REVIEW</b>           |       |
| 2.1 Introduction .....                         | 9     |
| 2.2 Fundamental properties of InN thin films   |       |
| 2.2.1 Structural properties .....              | 9     |
| 2.2.2 Optical and vibrational properties ..... | 12    |
| 2.2.3 Electrical properties .....              | 14    |

|       |   |    |
|-------|---|----|
| 2.3   | Challenges and fabrication methods of InN thin films              |    |
| 2.3.1 | Metal-organic chemical vapor deposition (MOCVD) .....             | 16 |
| 2.3.2 | Molecular beam epitaxy (MBE) .....                                | 19 |
| 2.3.3 | Radio-frequency (RF) sputtering .....                             | 21 |
| 2.3.4 | Hydride vapor phase epitaxy (HVPE) .....                          | 23 |
| 2.3.5 | Other growth methods .....  | 24 |
| 2.4   | An overview on sol-gel spin coating method .....                  | 25 |
| 2.5   | Factors influencing sol-gel spin coating growth of InN thin films |    |
| 2.5.1 | Substrates .....  | 29 |
| 2.5.2 | Buffer layers .....   | 32 |
| 2.5.3 | Nitridation conditions .....                                      | 33 |
| 2.6   | Applications  |    |
| 2.6.1 | Metal-semiconductor-metal (MSM) infrared photodetectors ...       | 37 |
| 2.7   | Summary .....   | 44 |

### **CHAPTER 3 – METHODS AND INSTRUMENTATION**

|       |  |    |
|-------|--|----|
| 3.1   | Introduction .....   | 45 |
| 3.2   | Growth of InN thin films using sol-gel spin coating method and nitridation |    |
| 3.2.1 | Sample and precursor preparations .....                                    | 45 |
| 3.2.2 | Nitridation process of sol-gel spin coated thin films .....                | 47 |
| 3.2.3 | Synthesis and optimizations of experiment conditions .....                 | 49 |
| 3.3   | Fabrication of MSM photodetector .....                                     | 50 |
| 3.4   | Principle of characterization systems                                      |    |
| 3.4.1 | High resolution X-ray diffraction (HR-XRD) .....                           | 51 |

|       |  |    |
|-------|--|----|
| 3.4.2 | Field-emission scanning electron microscopy (FESEM) .....  | 54 |
| 3.4.3 | Energy dispersive X-ray spectroscopy (EDS) .....   | 55 |
| 3.4.4 | Fourier transform infrared (FTIR) spectroscopy .....   | 56 |
| 3.4.5 | Raman spectroscopy .....   | 58 |
| 3.4.6 | Ultraviolet-visible-near infrared (UV-Vis-NIR) spectroscopy ..   | 59 |
| 3.4.7 | Current-voltage (I-V) characteristics and photoresponse<br>measurements of MSM IR photodetectors ..... | 61 |
| 3.5   | Summary .....  | 63 |

## **CHAPTER 4 – RESULTS AND DISCUSSION: PRECURSOR**

### **PREPARATION, SYNTHESIS, AND**

### **CHARACTERIZATIONS OF INDIUM NITRIDE THIN**

### **FILMS WITH DIFFERENT GROWTH PARAMETERS**

|       |   |    |
|-------|---|----|
| 4.1   | Introduction .....  | 64 |
| 4.2   | Preparation of indium-containing precursor                                      |    |
| 4.2.1 | UV-Vis transmission .....   | 65 |
| 4.3   | Effects of nitridation temperature on the sol-gel spin coated InN thin<br>films |    |
| 4.3.1 | Crystalline structure .....   | 65 |
| 4.3.2 | Surface morphology and elemental composition analysis .....                     | 70 |
| 4.3.3 | Optical properties .....  | 73 |
| 4.4   | Effects of nitridation duration on the sol-gel spin coated InN thin films       |    |
| 4.4.1 | Crystalline structure .....   | 76 |
| 4.4.2 | Surface morphology and elemental composition analysis .....                     | 80 |
| 4.4.3 | Optical properties .....  | 88 |

|       |   |     |
|-------|---|-----|
| 4.5   | Effects of thermal decomposition of ammonia gas on the sol-gel spin coated InN thin films |     |
| 4.5.1 | Crystalline structure .....   | 85  |
| 4.5.2 | Surface morphology and elemental composition analysis .....                               | 87  |
| 4.5.3 | Optical properties .....  | 90  |
| 4.6   | Effects of number of coating cycle on the sol-gel spin coated InN thin films              |     |
| 4.6.1 | Crystalline structure .....   | 95  |
| 4.6.2 | Surface morphology and elemental composition analysis .....                               | 99  |
| 4.6.3 | Optical properties .....  | 103 |
| 4.7   | Effects of the sol-gel spin coated InN thin film grown on GaN nucleation layer            |     |
| 4.7.1 | Crystalline structure .....   | 106 |
| 4.7.2 | Surface morphology and elemental composition analysis .....                               | 108 |
| 4.7.3 | Optical properties .....  | 109 |
| 4.8   | Summary .....   | 112 |
| .     |   |     |

**CHAPTER 5 – FABRICATION OF INDIUM NITRIDE-BASED MSM  
IR PHOTODETECTORS**

|     |                                       |     |
|-----|---------------------------------------|-----|
| 5.1 | Introduction .....                    | 114 |
| 5.2 | I-V characteristics measurement ..... | 114 |
| 5.3 | Photoresponses measurement .....      | 118 |
| 5.4 | Summary .....                         | 121 |

**CHAPTER 6 – CONCLUSIONS AND RECOMMENDATIONS FOR  
FUTURE WORK**

|     |                                       |     |
|-----|---------------------------------------|-----|
| 6.1 | Conclusions .....                     | 123 |
| 6.2 | Recommendations for future work ..... | 126 |

|                         |     |
|-------------------------|-----|
| <b>REFERENCES</b> ..... | 128 |
|-------------------------|-----|

**APPENDICES**

**LIST OF PUBLICATIONS**

## LIST OF TABLES

|           |  | <b>Page</b> |
|-----------|--|-------------|
| Table 2.1 | Experimental and theoretical Raman active modes for InN with wurtzite structure.   | 13          |
| Table 2.2 | General properties of wurtzite structure InN.  | 14          |
| Table 2.3 | Important parameter of reported nanostructured InN-based IR photodetector.   | 43          |
| Table 3.1 | Experiment conditions in synthesizing InN thin films on AlN templates.   | 53          |
| Table 4.1 | Lattice parameters and strains for the InN thin films deposited at various nitridation durations.  | 79          |
| Table 4.3 | Lattice parameters and strains for the InN thin films at various coating cycles.   | 99          |
| Table 4.4 | Lattice parameters and strains of the sol-gel spin coated InN thin films grown on AlN templates: (a) without, and (b) with GaN nucleation layer.             | 108         |
| Table 4.5 | Comparison of $E_g$ values obtained from experimental and reported InN grown on various substrates.  | 112         |
| Table 5.1 | Characteristics of the InN-based MSM IR photodetectors fabricated: (a) without, and (b) with GaN nucleation layer under dark and IR illumination conditions. | 117         |
| Table 5.2 | Comparison of rise and decay times obtained from experimental and reported work at different voltages.   | 119         |

## LIST OF FIGURES

|            |  | <b>Page</b> |
|------------|--|-------------|
| Figure 2.1 | Atomic arrangement of: (a) zinc-blende, (b) wurtzite, and (c) rock-salt structures. Open circle, closed circle, and solid line (thick) represent anion ( $N^-$ ), cation ( $In^+$ ) and projection of two bonds, respectively. | 11          |
| Figure 2.2 | Stacking model of wurtzite InN unit cell.  | 11          |
| Figure 2.3 | Energy band gap and lattice constant of the materials that used as substrate and intermediate layer for the growth of InN epilayers.   | 29          |
| Figure 2.4 | Schematic diagram of: (a) <i>p-n</i> junction photodiode structure and (b) I-V characteristics for dark current and illuminated conditions of photodiode.  | 37          |
| Figure 2.5 | Photocurrent mechanism of QWIP.  | 39          |
| Figure 2.6 | MSM structure photodetector equivalents to two Schottky diodes connected back-to-back.   | 40          |
| Figure 2.7 | Energy-band diagram of a biased MSM photodetector, indicating (1) photo-generated signal charges and (2) thermally-generated carriers overcoming barrier heights, which contribute to device dark current.                     | 40          |
| Figure 2.8 | Energy-band diagram of a metal and <i>n</i> -type semiconductor illustrating the carrier transport mechanism.  | 41          |
| Figure 2.9 | Different current transport mechanism in metal-semiconductor Schottky diodes.  | 42          |
| Figure 3.1 | Plasma system (PlasmaPrep 100) used for substrate surface treatment.   | 46          |
| Figure 3.2 | Spin coater system (GLICHN Technology, T-108 model) used for thin film deposition.   | 47          |
| Figure 3.3 | (a) Schematic diagram of the tube furnace system used for nitridation process. (b) The tube furnace system used for nitridation process.   | 48          |
| Figure 3.4 | Flow chart of the research work.   | 49          |

|             |   |    |
|-------------|---|----|
| Figure 3.5  | RF sputtering system (Edwards A500) used for metal contact deposition.  | 50 |
| Figure 3.6  | Schematic structures of (a) MSM metal mask, and InN-based photodetector (b) without, and (c) with GaN nucleation layer.   | 50 |
| Figure 3.7  | Geometry for the wave interference at a spacing $d$ .   | 52 |
| Figure 3.8  | HR-XRD system (PANalytical X'Pert PRO MRD PW3040).  | 53 |
| Figure 3.9  | FESEM system attached with EDS (NOVA NANOSEM 450).  | 54 |
| Figure 3.10 | Schematic diagram of inner atomic electron shells denoted as K, M and L.  | 56 |
| Figure 3.11 | Optical layout of an FTIR spectroscopy.   | 57 |
| Figure 3.12 | FTIR system (Spectrum GX FT-IR, Perkin Elmer).  | 57 |
| Figure 3.13 | Raman system (Horiba Jobin Yvon HR 800 UV).   | 58 |
| Figure 3.14 | Energy-level diagram for Rayleigh and Raman scatterings.  | 59 |
| Figure 3.15 | UV-Vis-NIR system (Cary 5000 Spectrophotometer).  | 60 |
| Figure 3.16 | Relative energies of orbitals involved in electronic spectra of molecules.  | 60 |
| Figure 3.17 | Experimental setup for IR photodetection measurements.  | 61 |
| Figure 3.19 | Response speed of a device.   | 62 |
| Figure 4.1  | Transmission of the precursor versus wavelength.  | 65 |
| Figure 4.2  | XRD patterns of the deposited thin films: (a) before, and after 45 min nitridation at (b) 500, (c) 550, (d) 600, and (e) 650 °C.  | 66 |
| Figure 4.3  | Low-magnification ( $\times 10$ k) FESEM images of the deposited thin films: (a) before nitridation, and after nitridation at (b) 500, (c) 550, (d) 600, and (e) 650 °C. Inset shows the cross-sectional images at high-magnification ( $\times 80$ k). | 71 |
| Figure 4.4  | EDS of the deposited InN thin films: (a) before   | 72 |

nitridation, and after nitridation at (b) 500, (c) 550, (d) 600, and (e) 650 °C.

|             |   |    |
|-------------|---|----|
| Figure 4.5  | IR reflectance spectra of the InN thin films nitrided at (a) 550, and (b) 600 °C for 45 min.  | 73 |
| Figure 4.6  | Raman spectra of the deposited thin films after nitridation temperature at (a) 550 and (b) 600 °C for 60 min.   | 75 |
| Figure 4.7  | XRD patterns of the deposited thin films at nitridation duration of: (a) 30, (b) 45, and (c) 60 min at 600 °C.  | 77 |
| Figure 4.8  | FWHM (■) and crystallite size (Δ) extracted from the InN(101) diffraction peak of the samples nitrided at: (a) 30, (b) 45, and (c) 60 min.  | 78 |
| Figure 4.9  | Low-magnification (×10 k) FESEM images of the deposited thin films at nitridation duration of: (a) 30, (b) 45, and (c) 60 min. Inset shows the cross-sectional FESEM images at high-magnification (×80 k).                                      | 81 |
| Figure 4.10 | EDS of the deposited thin films at nitridation duration of: (a) 30, (b) 45, and (c) 60 min.   | 82 |
| Figure 4.11 | IR reflectance spectra of the deposited InN thin films at nitridation duration of: (a) 30, (b) 45, and (c) 60 min.  | 83 |
| Figure 4.12 | Raman spectra of the deposited InN thin films at nitridation duration of: (a) 45 and (b) 60 min at 600 °C.  | 84 |
| Figure 4.13 | XRD patterns of the deposited InN thin films at thermal decomposition of NH <sub>3</sub> gas of: (a) 700, (b) 750, (c) 800, and (d) 850 °C.   | 86 |
| Figure 4.14 | Low magnification (×10 k) FESEM images of the deposited InN thin films at thermal decomposition of NH <sub>3</sub> gas: (a) 700, (b) 750, (c) 800, and (d) 850 °C. Inset shows the cross-sectional FESEM images at high magnification (×200 k). | 88 |
| Figure 4.15 | Elemental analysis of the deposited InN thin films at thermal decomposition of NH <sub>3</sub> gas: (a) 700, (b) 750, (c) 800, and (d) 850 °C.  | 89 |
| Figure 4.16 | IR reflectance spectra of the InN deposited thin films  | 91 |

at thermal decomposition of NH<sub>3</sub> gas: (a) 700, (b) 750, (c) 800, and (d) 850 °C.

|              |  |     |
|--------------|--|-----|
| Figure 4.17  | Raman spectra of the deposited InN thin films at thermal decomposition of NH <sub>3</sub> gas: (a) 700, (b) 750, (c) 800, and (d) 850 °C.  | 92  |
| Figure 4.18  | Graphical representation of Kubelka-Munk: $[h\nu F(R_\infty)]^2$ versus $h\nu$ (eV).   | 95  |
| Figure 4.19  | XRD patterns of the sol-gel spin coated InN thin films at various coating cycles: S1 (10), S2 (20), and S3 (30).   | 96  |
| Figure 4.20  | Schematic diagram illustrates growth process of InN thin films.  | 97  |
| Figure 4.21  | FWHM (▲) and crystallite size (■) extracted from the InN(101) diffraction peak of the samples coated at various coating cycles.  | 98  |
| Figure 4.22  | FESEM images (×10 k) of the InN thin films at various coating cycles: 10 (S1), 20 (S2), and 30 (S3). Inset shows the cross-sectional images recorded at different magnifications, scale bars are inserted for reference. | 100 |
| Figure 4.23  | Film thickness of the InN thin films at various coating cycles: 10 (S1), 20 (S2), and 30 (S3).   | 101 |
| Figure 4.24  | EDS elemental analysis of the InN thin films at various coating cycles: 10 (S1), 20 (S2), and 30 (S3).   | 102 |
| Figure 4.25: | Raman spectra of the deposited thin films at various coating cycles: (a) 10 (S1), (b) 20 (S2), and (c) 30 (S3).  | 104 |
| Figure 4.26  | Graphical representation of Kubelka-Munk: $[h\nu F(R_\infty)]^2$ versus $h\nu$ (eV) in range of 1.5 to 2.0 eV for the samples coated at 10 (S1), 20 (S2), and 30 (S2).   | 105 |
| Figure 4.27  | XRD patterns of: (a) GaN on AlN template, and (b) InN film grown on AlN template with GaN nucleation layer.  | 106 |
| Figure 4.28  | (a) High magnification (×100 k) FESEM image, and (b) elemental analysis of the InN thin film grown on  | 109 |

AlN template with GaN nucleation layer.

|             |   |     |
|-------------|---|-----|
| Figure 4.29 | Raman spectra of InN thin film deposited on AlN template with GaN nucleation layer.   | 110 |
| Figure 4.30 | Graphical representation of Kubelka-Munk: $[h\nu F(R_\infty)]^2$ versus $h\nu(\text{eV})$ .   | 111 |
| Figure 5.1  | Log $I$ - $V$ characteristics of the InN thin films grown on AlN templates: (a) without and (b) with GaN nucleation layer under the dark and IR illumination conditions. Inset shows $I$ - $V$ characteristics of the samples ranging from -10 to 10 V. | 116 |
| Figure 5.2  | Photoresponse properties of the InN thin films grown on AlN templates: without [(a), (b), and (c)], and with GaN nucleation layer [(d), (e), and (f)] at bias voltages of 1, 3, and 5.  | 119 |
| Figure 5.3  | Responsivity as a function of bias voltage for the InN thin films grown on AlN template: (a) without, and (b) with GaN nucleation layer.  | 121 |

## LIST OF SYMBOLS

|                           |   |
|---------------------------|---|
| $\alpha$                  | Absorption coefficient                    |
| $k$                       | Boltzmann constant                        |
| $\theta$                  | Bragg's angle                             |
| $\tau$                    | Crystallite size                          |
| $I$                       | Current                                   |
| $\epsilon_0$              | Dielectric function                       |
| $\delta$                  | Dislocation density                       |
| $d$                       | Distance between adjacent planes of atoms |
| $m_{eff}$                 | Effective mass                            |
| $q$                       | Elementary charge                         |
| $d_f$                     | Film thickness                            |
| $N$                       | Free-charge carrier concentration         |
| $\nu$                     | Frequency of vibration                    |
| $\beta$                   | Full-width at half-maximum                |
| $\epsilon_\infty$         | High frequency dielectric permittivity    |
| $n$                       | Ideality factor                           |
| $P_{opt}$                 | Incident optical power                    |
| $\epsilon_{yy}$           | In-plane strain                           |
| $F(R_\infty)$             | Kubelka-Munk function                     |
| $a, c$                    | Lattice constants                         |
| $h, k, i, \text{ and } l$ | Miller-Bravais indices                    |

|                                |   |
|--------------------------------|---|
| $E_g$                          | Energy band gap                         |
| $\pi(\sigma), \pi^*(\sigma^*)$ | Orbitals of conjugated functional group |
| $n_r$                          | Order number of the reflection planes   |
| $\varepsilon_{zz}$             | Out-of-plane strain                     |
| $\Delta p$                     | Partial pressure difference             |
| $Q$                            | Permeability coefficient                |
| $I_{ph}$                       | Photocurrent                            |
| $h$                            | Planck constant                         |
| $\omega_p$                     | Plasma frequency                        |
| $z, \dot{z}, x$                | Porto's notation                        |
| $A$                            | Proportional constant                   |
| $R$                            | Reflectance                             |
| $R_s$                          | Responsivity                            |
| $A^*$                          | Richardson coefficient                  |
| $I_0$                          | Saturation current                      |
| $\Phi_B$                       | Schottky barrier height                 |
| $A_{SC}$                       | Schottky contact area                   |
| $K$                            | Shape-factor                            |
| $a_0, c_0$                     | Strain-free lattice constants           |
| $A_s$                          | Surface area                            |
| $T$                            | Temperature                             |
| $t$                            | Time                                    |

|                  |   |
|------------------|---|
| $\omega_{TO/LO}$ | Uncoupled TO/LO phonon mode frequencies |
| $V$              | Voltage                                 |
| $\lambda$        | Wavelength                              |

## LIST OF ABBREVIATIONS

|                |   |
|----------------|---|
| <i>a</i> -axis | <i>a</i> -plane crystallographic axis       |
| R–O            | Alkoxy group                                |
| <i>c</i> -axis | <i>c</i> -plane crystallographic axis       |
| I-V            | Current-voltage                             |
| ECR            | Electron cyclotron resonance                |
| EDS            | Energy X-ray dispersive spectroscopy        |
| FE             | Field emission                              |
| FESEM          | Field-emission scanning electron microscopy |
| FTIR           | Fourier transform IR                        |
| FWHM           | Full-width at half-maximum                  |
| GZO            | Gallium-doped zinc oxide                    |
| HR-XRD         | High-resolution X-ray diffraction           |
| HPCVD          | Hybrid physical-chemical vapor deposition   |
| HVPE           | Hydride vapor phase epitaxy                 |
| R–OH           | Hydroxyl                                    |
| IR             | Infrared                                    |
| JCPDS          | International Centre for Diffraction Data   |
| LPP            | LO phonon-plasmon coupling                  |
| LO             | Longitudinal optical                        |
| LT-            | Low temperature-                            |
| MOCVD          | Metal-organic chemical vapor deposition     |
| MOMBE          | Metal-organic molecular beam epitaxy        |
| MOVPE          | Metal-organic vapor phase epitaxy           |

|            |   |
|------------|---|
| MSM        | Metal-semiconductor-metal               |
| MBE        | Molecular beam epitaxy                  |
| PL         | Photoluminescence                       |
| PLE        | Photoluminescence excitation            |
| PVDNC      | Plasma vapor deposition of nano-columns |
| PLD        | Pulsed laser deposition                 |
| QWIP       | Quantum-well infrared photodetector     |
| RF         | Radio-frequency                         |
| SBH        | Schottky barrier height                 |
| TE         | Thermionic emission                     |
| TFE        | Thermionic field emission               |
| TO         | Transverse optical                      |
| TMI        | Trimethylindium                         |
| UV         | Ultraviolet                             |
| UV-Vis     | Ultraviolet-visible                     |
| UV-Vis-NIR | Ultraviolet-visible-near infrared       |

# **PERTUMBUHAN DAN PENCIRIAN FILEM NIPIS INDIUM NITRIDA MELALUI KAEDAH SALUTAN PUTARAN**

## **ABSTRAK**

Indium nitrida (InN) telah menerima perhatian penyelidik dan industri pembuatan kerana ciri-ciri uniknya seperti jurang jalur tenaga yang sempit 0.7 – 1.0 eV, kelincahan elektron yang tinggi dan kepekatan pembawa yang rendah. Walau bagaimanapun, hanya terdapat sedikit kerja-kerja mengenai mekanisme pertumbuhan filem nipis InN, ini disebabkan suhu penguraian InN yang rendah dan ketidakpadanan-kekisi antara filem dan substrat. Dengan ini, hanya terdapat sedikit kerja-kerja terperinci mengenai filem nipis InN yang telah dilaporkan. Teknik pemendapan seperti pemendapan wap kimia logam organik, epitaksi alur molekul dan pemercikan frekuensi-radio telah digunakan untuk mensintesis InN. Walau bagaimanapun, teknik-teknik ini memerlukan sistem vakum ultra tinggi, pelopor toksik serta setup yang mahal dan rumit. Dalam kerja ini, pertumbuhan, pencirian dan aplikasi peranti filem nipis InN yang ditumbuhkan di atas templat aluminium nitrida (AlN) melalui kaedah salutan putaran sol-gel dan diikuti dengan proses penitridaan telah dikaji. Fasa awal kerja ini adalah untuk menentukan suhu penitridaan dan tempoh yang sesuai untuk pertumbuhan filem nipis InN. Filem disalutkan sol-gel (indium nitrat hidrat) telah dinitrida dalam keadaan ammonia ( $\text{NH}_3$ ) pada suhu pertumbuhan antara 550 – 700 °C selama 30 – 60 min. Melalui kajian-kajian ini, didapati bahawa keadaan optima untuk pertumbuhan filem nipis InN adalah 600 °C dan 45 min, juga, ditentukan bahawa kerjayaan pertumbuhan InN memerlukan pembentukan indium oksida ( $\text{In}_2\text{O}_3$ ). Selepas itu, kesan terma

penguraian gas  $\text{NH}_3$  daripada 700 – 850 °C ke atas pertumbuhan kristal InN telah dikaji. Pada suhu yang tinggi ( $> 700$  °C), penguraian InN dan kesan punaran terma telah diperhatikan disebabkan peningkatan tekanan separa hidrogen di dalam sistem. Selain itu, ketebalan filem boleh dikawal dengan mengubah bilangan kitaran salutan (iaitu 10, 20, dan 30 kitaran). Didapati bahawa penukaran lengkap  $\text{In}_2\text{O}_3$  kepada InN tidak tercapai sepenuhnya apabila ia mencapai ketebalan kritikal sebanyak 2.39  $\mu\text{m}$ , menyebabkan pembentukan fasa campuran  $\text{In}_2\text{O}_3$  dan InN kristal. Untuk mengurangkan ketidakpadanan kekisi antara InN dan AlN-templat, lapisan penukleusan GaN telah digunakan. Keputusan menunjukkan InN filem berorientasi-*c* telah diperolehi, manakala jurang jalur tenaga telah dikurangkan daripada 1.72 eV dengan tanpa lapisan penukleusan GaN kepada 1.70 eV. Aplikasi pengesan cahaya bagi filem nipis InN salutan sol-gel di atas AlN-templat dengan dan tanpa lapisan penukleusan GaN juga telah dikaji dengan menfabrikasi fotopengesan inframerah logam-semikonduktor-logam. Peranti tersebut menunjukkan kepekaan yang baik dan keterulangan terhadap pengujian inframerah pada panjang gelombang 808 nm. Metodologi yang dicadangkan memberikan idea baru untuk menghasilkan peranti semikonduktor berasaskan InN dengan menggunakan teknik pemendapan yang ringkas dan kos-rendah.

# SPIN COATING GROWTH AND CHARACTERIZATION OF INDIUM NITRIDE THIN FILMS

## ABSTRACT

Indium nitride (InN) has received attention of researchers and manufacturing industry because of its unique properties such as narrow energy band gap of 0.7 – 1.0 eV, high electron mobility and low carrier concentration. However, there is relatively few reported studies concerning the growth mechanism of InN, due to the low dissociation temperature of InN and large lattice-mismatch between the film and substrate. The deposition techniques such as metal-organic chemical vapor deposition, molecular beam epitaxy and radio-frequency sputtering have been used to synthesize InN. However, these techniques require an ultrahigh vacuum system, a toxic precursor as well as a relatively expensive and complicated setup. In this work, the growth, characterization, and device application of InN thin films grown on aluminium nitride-template through sol-gel spin coating method followed by nitridation process were studied. The initial phase of this work is to determine the suitable nitridation temperature and duration for the growth of InN thin film. The sol-gel spin coated film (indium nitrate hydrate) was nitrided in ammonia (NH<sub>3</sub>) ambient at growth temperature ranged 550 – 700 °C for 30 – 60 min. Through these studies, it was found that the optimal conditions for the growth of InN thin film are 600 °C and 45 min, also, it can be determined that the successful growth of InN requires a formation of indium oxide (In<sub>2</sub>O<sub>3</sub>). Subsequently, the effects of thermal decomposition of NH<sub>3</sub> gas ranging from 700 – 850 °C on InN crystal growth were studied. At the high temperature (> 700 °C), the dissociation of InN and thermal

etching effect were observed which due to the increase of partial pressure of hydrogen in the system. Furthermore, the film thickness can be controlled by varying the number of coating cycles (i.e. 10, 20, and 30 cycles). It was found that the complete conversion of  $\text{In}_2\text{O}_3$  into InN was not fully achieved when it reached a critical thickness of about  $2.39 \mu\text{m}$ , causing the formation of mixed phase of  $\text{In}_2\text{O}_3$  and InN crystals. To reduce the lattice mismatch between InN and AlN-template, a GaN nucleation layer was applied. The results showed the *c*-preferred orientation InN thin film was obtained, while energy band gap was reduced from 1.72 eV without GaN nucleation layer to 1.70 eV. The light sensing application of the sol-gel spin coated InN thin films on AlN-template with and without GaN nucleation layer was also studied by fabricating metal-semiconductor-metal infrared photodetectors. These devices demonstrated a good sensitivity and repeatability towards the infrared excitation at wavelength 808 nm. The proposed methodology suggests a new idea to produce InN-based semiconductor devices using a relatively simple and low-cost deposition technique.

# CHAPTER 1

## INTRODUCTION

### 1.1 Introduction

Group III-nitride compounds such as indium nitride (InN), gallium nitride (GaN) and aluminium nitride (AlN) have received substantial research and industrial interests. These materials are fascinating because of their direct band gap which covers the range of 0.7 to 6.2 eV. In particular, InN is of considerable interest due to its outstanding properties such as a narrow band gap of 0.7 to 1.0 eV, high electron mobility, and low effective mass at room temperature (Chen et al., 2012a). These characteristics fulfill the requirements for the applications of high-speed and high-performance InN-based optical and electronic semiconductor devices. Since then, the devices such as light-emitting diodes, high efficiency solar cells, laser diodes, terahertz emitters, and high frequency transistors operating at high power and temperature have been developed, as to improve the conventional semiconductor technology (Stokker-Cheregi et al., 2013). In addition, the presence of electron accumulation on the InN surface leads to high surface sensitivity, hence a promising candidate for sensor applications (Ruffenach et al., 2010). Besides, the ternary III-nitrides such as indium gallium nitride ( $\text{In}_x\text{Ga}_{1-x}\text{N}$ ) and indium aluminium nitride ( $\text{In}_x\text{Al}_{1-x}\text{N}$ ) can be formed in the corporation of InN and its alloys with GaN and AlN, allowing the extension of light emission from ultraviolet (UV) to infrared (IR) region (Nakamura et al., 1993). Also, it was reported that the  $\text{In}_x\text{Ga}_{1-x}\text{N}$  and  $\text{In}_x\text{Al}_{1-x}\text{N}$  with tunable band gaps have the potential to be used in the fabrication of multi-junction solar cells (Yamamoto et al., 2013).

Despite the rapid development of InN-based semiconductor devices, fundamental challenges remain in developing high crystallinity InN thin films. The synthesis of InN is considered the most challenging among the III-nitride compounds. This is because the growth mechanism of InN is associated with various limitations which mainly due to the low dissociation temperature (around 630 °C), high volatility of atomic nitrogen, lack of lattice-matching substrates, and difficulty to prepare in stoichiometric form (MacChesney et al., 1970; Chen and Kuo, 2012). Several studies reported that the thermal stability is one of the critical factors affecting the InN crystal growth. At high growth temperatures, the metallic-indium tends to dissociate from the crystal. Thus, to prevent the thermal decomposition of InN, researchers proposed to grow InN epilayers at low temperatures (Gao et al., 2003; Chen et al, 2012b). However, the low growth temperature has resulted in the deficiency of active nitrogen (N) atoms and reduction of the kinetic energies of the reactants in forming InN bonds (Stokker-Cheregi et al., 2013).

A variety of advanced deposition techniques include metal-organic chemical vapor deposition (MOCVD), molecular beam epitaxy (MBE), plasma-assisted reactive evaporation, and reactive sputtering have been developed to fabricate high crystallinity InN thin films (Chen and Kuo, 2012; Tuna et al., 2011). Several studies reported that the MOCVD has been one of the major process in the semiconductor devices manufacturing industry. Although it is beneficial in large area deposition, excellent composition control and film uniformity, an essential requirement in this method is the availability of suitable precursor with sufficient volatility and stability. The crystallinity of MOCVD growth InN is strongly dependent on the V/III source ratio, where the lack of which source will lead to the formation of indium droplets (Jones, 1998; Tuna et al., 2011). On the other hand, the MBE growth is dependent

upon the atomic species being deposited. To overcome the problem of atomic impurities, an ultrahigh vacuum system is required to remove the unwanted background gases, such as oxygen, which causes defects on the deposited thin films (Mukundan et al., 2015). These conventional techniques are advantageous in obtaining high quality InN thin films, but relatively expensive and complicated setups are needed. Hence, a simple, safe, non-toxic, and cost effective deposition method to produce InN thin films is highly desirable.

Following the success of Fong et al. on the sol-gel spin coating growth of GaN thin films on silicon (Si) substrates (Fong et al., 2015), we propose that the technique can be applied to produce InN thin films. In general, the sol-gel spin coating is a dilute-solution based approach. It has been widely used in the deposition of doped and undoped metal oxides thin films because of the capability to control film thickness and morphology, relatively simple setup, low-cost, fast processing and environment-friendly (Bhatia et al., 2017; Talikder et al., 2016; Shaban et al., 2015). In literature, the sol-gel chemistry in producing nitride materials have been introduced over the past decades (Hector, 2007). However, to the best of our knowledge, the growth of InN thin films using sol-gel spin coating method has not been explored. The fundamental issues associated with the growth mechanism and materials properties still remain unknown. Therefore, in-depth investigations into factors that influence the InN crystal growth were performed. The properties of the deposited films were investigated using various characterization tools include high-resolution X-ray diffraction (HR-XRD), field-emission scanning electron microscopy (FESEM), energy X-ray dispersive spectroscopy (EDS), Fourier transform infrared (FTIR), and Raman spectroscopy. Apart from that, we extend the study by investigating the light sensing application of these sol-gel spin coated thin films through the fabrication of metal-semiconductor-

metal (MSM) IR photodetectors. As far as we know, there are few studies reported on the nanostructured InN-based IR photodetectors (Tekcan et al., 2014; Lai et al., 2010; Chen et al., 2009), and there is no publication on the sol-gel spin coated InN-based photodetector. Hence, we believe that the success of this study may contribute to the significant advancement of knowledge in materials science and thin film technology.

## **1.2 Motivation and problem statements**

InN is a semiconductor compound worthy of study because of the aforementioned unique properties and numerous potential applications. To date, there is relatively little detailed comparative works concerning the InN thin films due to their stringent suitable growth conditions. In order to obtain high quality InN films, a better understanding on the growth mechanism and material properties is necessary to enable selection of appropriate growth parameters. The sol-gel spin coating method followed by nitridation could be a viable technique for the deposition of InN thin films because of its several advantages compared to the conventional techniques. This approach allows the deposition at low temperature range, easy in handling, cost effective, and fast processing.

Establishing a promising methodology requires in-depth investigations into the factors that influence the material properties of the sol-gel spin coated InN films. Thermal stability of InN has long been a critical issue in affecting the crystal growth by which thermal dissociation of InN and desorption of nitrogen atoms can be easily occurred at high temperature, causing the formation of metallic-In and indium (III) oxide ( $\text{In}_2\text{O}_3$ ). Therefore, a study on the effects of growth temperature is necessary to determine the suitable temperature range for the sol-gel spin coating growth of InN

films. In addition, a study on nitridation duration is performed to determine the transformation stage of the sol-gel spin coated film into InN phase. Inappropriate growth conditions could lead to film agglomeration, and decrease the device performance. During the nitridation process, the supplied ammonia ( $\text{NH}_3$ ) gas is decomposed into reactive nitrogen and hydrogen atoms. The decomposition temperature is closely related to the dissociation rate of  $\text{NH}_3$  gas. Thus, understanding in the thermal decomposition of  $\text{NH}_3$  gas and the effects of hydrogen atoms provides information in explaining the growth mechanism of InN thin films. Subsequently, the study on various number of coating cycles and application of GaN nucleation layer are performed to improve the quality of the InN thin films.

Furthermore, the fabrication and characterization of the sol-gel spin coated InN-based MSM IR photodetectors are carried out. Up to now, the proposed methodology has not been reported in literature, hence, this topic is worthy to explore. The findings describe in this dissertation could be beneficial to the research field and industry in terms of providing a significant knowledge on the novel deposition technique, also, may contribute to the advancement of future semiconductor device technology.

### **1.3 Research objectives**

The primary objective of this research is to synthesize InN thin films on AlN templates through sol-gel spin coating method followed by nitridation process. The growth mechanism and fundamental material properties of the sol-gel spin coated InN thin films are determined. The characterization tools such as HR-XRD, FESEM, EDS,

FTIR, and Raman spectroscopy will be used to analyze the surface morphologies, crystalline structure, and optical properties of the deposited films.

In-depth investigations into factors that influence the sol-gel spin coating growth of InN films will also be carried out. Various experiment conditions including nitridation temperature, nitridation duration, thermal decomposition of  $\text{NH}_3$  gas, number of coating cycle, and application of GaN nucleation layer will be studied.

Finally, the sol-gel spin coated InN-based MSM IR photodetectors will be fabricated. The current-voltage (I-V) characteristics and photoresponse of these devices upon exposure to IR excitation at wavelength 808 nm will be investigated.

#### **1.4 Originality**

For the first time, the growth, characterizations, and device application of InN thin films using sol-gel spin coating method followed by nitridation process are reported. The thermal stability of InN has been a long-standing issue resulting in the stringent growth conditions. In this project, a relatively simple, low-cost and fast-processing sol-gel spin coating method is proposed as an alternative to the conventional deposition techniques. A custom-made system connecting two tube-furnaces is suggested to provide an independent control of growth and  $\text{NH}_3$  gas decomposition temperatures. The suitable range of growth temperature and duration are investigated, as well as the growth mechanism is revealed. Additionally, several factors that have major influences on the material properties of the sol-gel spin coated InN thin films are studied. Apart from that, considering the application of these sol-gel spin coated InN thin films has not been explored, the MSM IR photodetectors are

fabricated. Detailed analyses on the I-V characteristics and photoresponses of these devices under IR excitation are included in this dissertation.

## **1.5 Dissertation organization**

The content of the dissertation will be organized in several chapters. The dissertation begins with a brief introduction and research objectives.

Chapter 2 describes the fundamental properties of the InN thin films. In addition to the principle of sol-gel spin coating method, other major fabrication approaches are reviewed. Factors such as substrates, buffer layers, and nitridation conditions that influence InN crystal growth are emphasized. Lastly, the potential application of the sol-gel spin coated InN-based IR photodetectors is introduced.

Chapter 3 presents the research methodologies of this project, including the sample and precursor preparations, thermal nitridation, as well as the fabrication of photodetectors. A series of experiment conditions to optimize the InN thin films are also explained. Thereafter, the basic principles of the characterization systems such as HR-XRD, FESEM, EDS, FTIR, Raman, ultraviolet-visible (UV-Vis) spectroscopies, I-V and photoresponse measurements setups are described.

Chapter 4 reports the effects of nitridation temperature and duration on the surface morphologies, crystalline structure, and optical properties of the sol-gel spin coated InN thin films. The growth mechanism and chemical reaction involve in the InN crystal growth are discussed. Further, the substantive findings drawn from the optimization conditions include thermal decomposition of  $\text{NH}_3$  gas, number of coating cycles and application of GaN nucleation layer are discussed.

Chapter 5 presents the I-V characteristics and photoresponse of the sol-gel spin coated InN-based MSM IR photodetectors. The responsivity of these devices towards IR excitation are evaluated.

The thesis concludes with a discussion on the significant findings of this project and suggestions for future research in Chapter 6.

## **CHAPTER 2**

### **LITERATURE REVIEW**

#### **2.1 Introduction**

In recent years, there has been a remarkable progress in the development of InN-based optical and electrical semiconductor devices owing to their unique properties. Despite, the growth of InN thin films is considered the most challenging among the III-nitride compounds due to the stringent suitable growth conditions. In this chapter, the fundamental properties of the InN thin films are presented. In addition to the sol-gel spin coating technique, other fabrication approaches are reviewed. Thereafter, factors that influence the sol-gel spin coating growth of InN thin films are emphasized. Furthermore, the applications of the InN thin films are evaluated.

#### **2.2 Fundamental properties of InN thin films**

##### **2.2.1 Structural properties**

The binary compound of InN crystallizes in three phases, including wurtzite (hexagonal), zinc-blende (cubic), and rock-salt (Acharya, 2013). The main difference between wurtzite and zinc-blende structures is the stacking sequence in a unit cell. The stacking sequences in wurtzite along [0001] direction and zinc-blende along [001] direction are ABAB and ABCABC, respectively, where A, B, and C are denoted as the allowed sites of In-N pairs. Figure 2.1 shows the atomic arrangement of the phases. In a fault stacking, one structure can be transformed into another or create a structural

defect (Bügler, 2013). Both the phases can be synthesized depending on the crystallite structure of the applied substrates and the growth conditions. On the other hand, it is reported that the phase transition from wurtzite to rock-salt is occurred at a certain high pressure, such as 12.1 GPa (Morkoç, 2009). In general, the wurtzite exhibits the more thermodynamically stable than the zinc-blende. Therefore, in this work, only the wurtzite phase is investigated.

In literature, there has been a lot of controversy over the lattice properties of wurtzite structure InN. Transley and Foley reported that the radio-frequency (RF) sputtered InN film having the lattice parameter  $a = 3.548 \text{ \AA}$  and  $c = 5.760 \text{ \AA}$  (Tansley and Foley, 1986). However, the reported values were different from Kubota et al. where  $a = 3.540 \text{ \AA}$  and  $c = 5.705 \text{ \AA}$  (Kubota et al., 1989). These lattice parameters obtained by Kubota et al. were found to be comparable with that measured by Davydov et al.,  $a = 3.536 \text{ \AA}$  and  $c = 5.704 \text{ \AA}$  in the high-quality wurtzite InN film (Davydov et al., 2002a). All the lattice parameters are closed to the theoretical values of  $a = 3.501$  to  $3.536 \text{ \AA}$  and  $c = 5.69$  to  $5.705 \text{ \AA}$  (Bhuiyan et al., 2003), except for that reported by Transley and Foley. It was explained that the deviation is due to the discrepancy in the InN crystalline quality and incorporation of oxygen contamination (Yamamoto et al., 2006). Therefore, it can be deduced that the  $a$ -lattice parameters are to be in the range of  $a = 3.50$  to  $3.54 \text{ \AA}$ , and  $c$ -lattice parameters are in the range of  $c = 5.69$  to  $5.71 \text{ \AA}$ . Furthermore, the wurtzite structure of InN is defined as a member of the space group of  $P6_3\text{Mac}$  ( $C_{6v}^4$ ) (Sahoo et al., 2008). It has four atoms in a primitive cell, and it can be seen as a superposition of two body-centered zinc-blende sub lattices shifted against each other in the  $c$ -axis, as shown in Figure 2.2. The strong electric field is present along the  $c$ -axis due to the lack of a center of symmetry and strong ionicity of the In-N bonds, and leading to the anisotropic effect (Bügler, 2013).

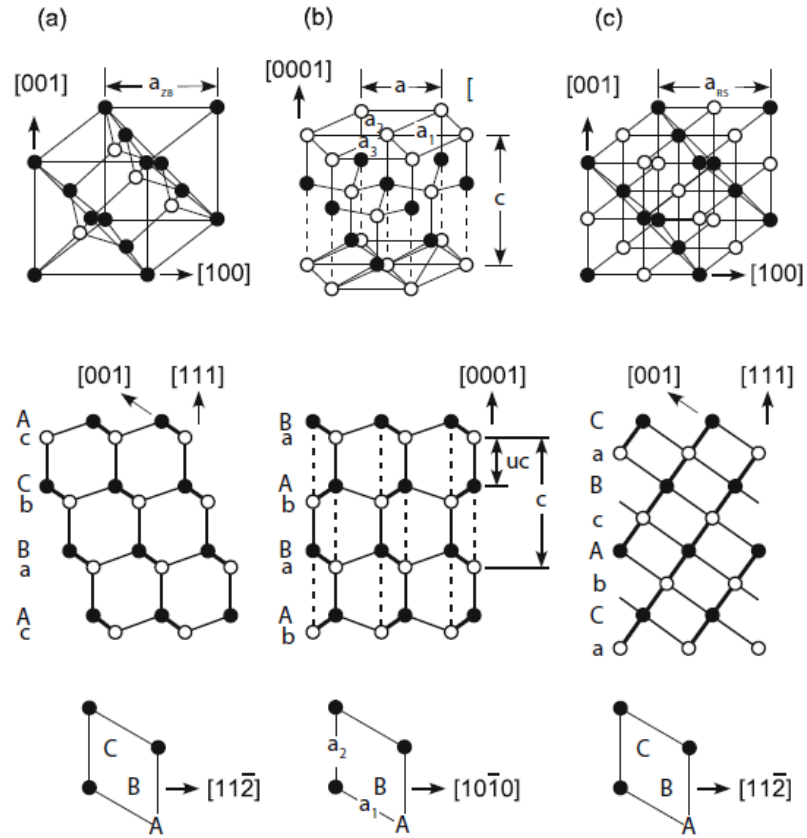


Figure 2.1: Atomic arrangement of: (a) zinc-blende, (b) wurtzite, and (c) rock-salt structures. Open circle, closed circle, and solid line (thick) represent anion ( $N^-$ ), cation ( $In^+$ ), and projection of two bonds, respectively [Adapted from Hanada, 2009].

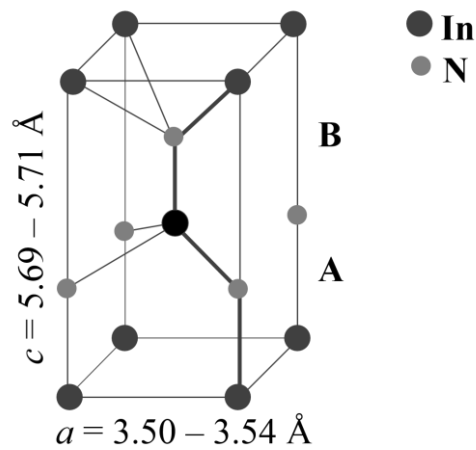


Figure 2.2: Stacking model of wurtzite  $InN$  unit cell [Reproduced from Morkoç, 2009].

### 2.2.2 Optical and vibrational properties

The fundamental physical properties of wurtzite structure InN have raised intense attention from researchers due to the controversy on the optical band gap of InN. In the early study, the commonly accepted band gap value for polycrystalline and nanocrystalline InN was in the range of 1.8 to 2.1 eV, which have usually been estimated from the absorption spectra (Tansley and Foley, 1986; Westra et al., 1988). Although the lowest energy band gap of InN around  $0.67 \pm 0.05$  eV was reported and this has generated a conflict with the previously accepted value (Walukiewicz et al., 2006). Researchers pointed out that the lower absorption edge is due to the presence of Mie resonances resulted from the inclusions of metallic-In in the InN matrix (Monemar et al, 2005). Davydov et al. later claimed that the slightly wider value of about 0.9 eV can be obtained for high quality InN thin films grown by MBE using techniques such as optical absorption, photoluminescence (PL), photoluminescence excitation (PLE), and ab initio calculations (Davydov et al., 2002b). In-depth investigations and analyses on band gap value of InN have been carried out through different measuring techniques such as optical absorption, PL and photomodulated reflection. These have successfully deduced that the low band gap of about 0.7 eV can be achieved through advancement in epitaxial growth techniques of InN thin films, by which the films with lower electron concentrations and higher electron mobility are desired (Nanishi et al, 2003).

Furthermore, the vibrational modes of InN can be identified through Raman and IR reflectance measurements (Ibáñez et al., 2011). The group symmetrical  $P6_{3Mac}$  ( $C_{6v}^4$ ) analysis of the wurtzite crystal structure of InN shows the six allowed optical modes including  $A_1$ ,  $E_1$ ,  $2E_2$ , and  $2B_1$ . The  $A_1$  and  $E_1$  are both Raman and IR active,

$E_2$  is only Raman active, and  $B_1$  is inactive in both Raman and IR. The polar  $A_1$  and  $E_1$  modes split into two components, such as longitudinal optical (LO) and transverse optical (TO) with different frequencies (Sahoo et al., 2008). Hence, there are in total of six Raman active modes can be observed, which are  $A_1(\text{LO})$ ,  $A_1(\text{TO})$ ,  $E_1(\text{LO})$ ,  $E_1(\text{TO})$ ,  $E_2(\text{high})$ , and  $E_2(\text{low})$ . Generally, the selection rule for vibrational modes depends on the symmetry of a molecule. The bands are considered Raman active when there is interaction between the electrons and nuclei as a result of the stretching and contraction of molecular bonds, causing the changes in polarizability (Sajan, 2007). The experimental and theoretical Raman active modes for the wurtzite structure of InN are summarized in Table 2.1.

Table 2.1: Experimental and theoretical Raman active modes for InN with wurtzite structure.

| <b>Experimental</b>      |                          |                            |                          |                          |                           |                           |
|--------------------------|--------------------------|----------------------------|--------------------------|--------------------------|---------------------------|---------------------------|
| <b>A<sub>1</sub>(TO)</b> | <b>E<sub>1</sub>(TO)</b> | <b>E<sub>2</sub>(high)</b> | <b>A<sub>1</sub>(LO)</b> | <b>E<sub>1</sub>(LO)</b> | <b>E<sub>2</sub>(low)</b> | <b>Reference</b>          |
| 448                      | 470                      | 485                        | 592                      |                          |                           | Bagavath et al., 2017     |
| 449                      | 476                      | 492                        | 595                      |                          | 88                        | Ibáñez et al., 2011       |
| 443                      | 475                      | 491                        | 591                      |                          |                           | Agulló-Rueda et al., 2000 |
| 436                      | 471                      | 488                        | 593                      | 572                      |                           | Wetzel and Akasaki, 1998  |
| <b>Theoretical</b>       |                          |                            |                          |                          |                           |                           |
| 443                      | 470                      | 492                        | 589                      | 605                      | 93                        | Kaczmarczyk et al., 2000  |

Agulló-Rueda et al. (2000) demonstrated the full-width at half-maximum (FWHM) of the  $E_2(\text{high})$  phonon mode was reduced from 13 to 7  $\text{cm}^{-1}$  with increasing growth temperature from 450 to 550 °C, indicating the improvement of InN

crystallinity. They explained that the peak broadening was induced by the lattice disorder due to the incorporation of impurities and defects.

### 2.2.3 Electrical properties

In general, the structural, optical and vibrational as well as electrical properties of wurtzite structure InN are summarized in Table 2.2. Studies show that InN is a promising III-V compound for the applications in high speed semiconductor devices due to the characteristics of small direct band gap energy, high electron mobility and saturation velocity (Hadi et al., 2013). For instance, light-emitting diodes, laser diodes, high efficiency solar cells, transistor, photodetectors as well as terahertz emitters (Xie et al., 2007; Nakamura et al., 1993).

Table 2.2: General properties of wurtzite structure InN.

| Properties                                 |                                       | References                  |
|--|---------------------------------------|-----------------------------|
| Space group                                | P6 <sub>3</sub> mc                    | Sahoo et al., 2008          |
| Lattice constant (Å)                       | 3.54 <sup>a</sup> , 5.71 <sup>c</sup> | Bhuiyan et al., 2003        |
| Band gap (eV)                              | 0.7 to 1.0                            | Nag, 2004; Xie et al., 2007 |
| Effective electron mass ( $m_{eff}$ )      | 0.06                                  | Acharya, 2013               |
| Electron concentration (cm <sup>-3</sup> ) | > 10 <sup>19</sup>                    |                             |
| Electron mobility (cm <sup>2</sup> /Vs)    | 3400                                  | O'Leary et al., 2010        |

*\*a and c refer to lattice constants.*

However, the surface electron accumulation effect in *n*-type InN reduces the potential in achieving *p-n* junction device, also prevents the formation of a rectifying

contact on InN (Lu et al., 2003c). InN has an unusual low conduction band minimum at the  $\Gamma$ -point of the Brillouin zone (Mahboob et al., 2004). This causes InN acts as donors which give rise to high background concentration of electrons. It is reported that this effect is dependent on surface reconstruction by which it can be modulated through external treatment using microwave hydrogen plasma (Noguchi et al., 1991).

The first attempt for synthesizing InN was performed in 1938, in which the wurtzite structure InN was successfully obtained from ammonium hexafluoroindate (III)  $[\text{InF}_6(\text{NH}_4)_3]$  (Juza et al., 1938). In later years, several works were carried out on the direct reaction of metallic-indium and nitrogen ( $\text{N}_2$ ) gas. However, the findings pointed out that the InN has not been made by this approach. Due to the stable phase of indium and  $\text{N}_2$ , it is very unfavorable to form InN at low temperatures. In fact, among the III-nitride compounds, only AlN has been formed in this manner. It is suggested that the rate limiting process can be improved by the reaction of In with atomic or excited nitrogen species (MacChesney et al., 1970). In subsequent, the reaction of In-compound with  $\text{NH}_3$  gas, or thermal dissociation of complex compound containing indium and nitrogen has successfully led to the formation of polycrystalline InN. The study reported that the obtained InN layer was highly conducting with electron concentration of around  $10^{18} \text{ cm}^{-3}$  (Hovel and Cuomo, 1972). Through the efforts of several research groups, the growth of good quality InN was successfully achieved in the late 1980s, mainly by sputtering (Tansley and Foley, 1986; Westra et al., 1988). A variety of advanced deposition techniques have been developed to obtain the high quality InN thin films, and realize the applications in semiconductor devices. These techniques include metal-organic chemical vapor deposition (MOCVD), molecular beam epitaxy (MBE), hydride vapor phase epitaxy

(HVPE), and radio-frequency (RF) sputtering. The details on the aforementioned growth techniques are discussed below.

## **2.3 Challenges and fabrication methods of InN thin films**

### **2.3.1 Metal-organic chemical vapor deposition (MOCVD)**

MOCVD also known as metal-organic vapor phase epitaxy (MOVPE), is one of the major processes in the manufacturing of semiconductor devices. This technique enables chemical vapor deposition of thin layers of atoms on flat substrates through chemical reaction. It is excellent for large-area deposition, composition control and film uniformity (Jones, 1998). The growth of single crystalline epitaxy InN was achieved by Matsuoka et al. via this approach in 1989, with the microwave-excited  $N_2$  gas (Matsuoka et al., 1990). In the MOCVD growth, the availability of suitable precursors with sufficient volatility and stability is important. The precursor needs to have the appropriate reactivity to decompose thermally (Neumayer and Ekerdt, 1996). For the synthesis of InN, the common materials such as trimethylindium (TMI) and  $NH_3$  were used as the indium and nitrogen sources, respectively. In addition,  $N_2$  can be used as a carrier gas to promote the thermal decomposition of  $NH_3$  gas during InN crystal growth (Ruffenach et al., 2010; Matsuoka et al., 2002).

Researchers pointed out that the InN crystal growth is dependent on the MOCVD growth parameters, such as temperature, V/III ratio, and vapor pressure of the sources (Yamamoto et al., 1994; Tuna et al., 2011). It was found that at the relatively low growth temperatures ( $< 400$  °C), the deposited thin film was dominated by metallic-In due to the lack of reactive N-atoms in the reactor. Thus, it was

concluded that the growth at the low temperatures was impossible because of the decreased migration of the deposited materials (Ruffenach et al., 2010; Kadys et al., 2015). Alternative approaches were proposed to promote the decomposition of  $\text{NH}_3$  gas, such as by laser-assisted activation and nitrogen plasma (Wintrebert-Fouquet et al., 2004). However, the findings showed the obtained poor crystalline quality of InN and metallic-In was observed (Yamamoto et al., 2006; Wintrebert-Fouquet et al., 2004). On the other hand, at the growth temperature of around 500 °C, both InN crystal growth and In-droplets can be observed. The authors suggested that the increase in temperature is able to promote thermal decomposition of  $\text{NH}_3$  gas and prevent the formation of metallic-In. However, further increase in temperature at around 600 to 650 °C has again caused to the formation of In-droplets. This phenomena was due to the nitrogen desorption effect which leaved the metallic-In on the film surface (Xie et al., 2007; Suihkonen et al., 2006). Hence, it can be deduced that the suitable temperature range for the MOCVD growth of InN is very stringent, at around 400 to 630 °C.

Although the growth rate could be enhanced with increasing temperature, at a constant V/III ratio and even a greater flow of TMI will lead to a saturation of InN formation, while the excess In-source will not able to form InN at the condition with limited nitrogen source. Several studies demonstrated that variation in V/III ratio has induced different growth modes and rates, and it is one of the important parameter in controlling the film properties (Jamil et al., 2008). Matsuoka (1997) showed that at the low growth temperatures ( $\leq 600$  °C), In-droplets were formed on a film surface at the V/III ratio lower than  $1.6 \times 10^4$ , while the In-droplet was not observed at increasing V/III ratio to more than  $1.6 \times 10^5$ . It is known that the decomposition rate of  $\text{NH}_3$  gas reduces with decreasing growth temperature. Hence, relatively high input V/III ratio

is needed to produce an adequate amount of reactive nitrogen source for the chemical reaction. On the other hand, the growth mechanism of InN is different at high growth temperatures (approximately 650 °C). The low input V/III ratio is required at high growth temperature, in which the dissociation of NH<sub>3</sub> gas is greatly enhanced. Koukitu et al. (1999) showed that the high decomposition rate of NH<sub>3</sub> gas has led to the increase of hydrogen partial pressure in the reactor, and reduce the driving force for the deposition. As a result, the occurrence of negative driving force will induce the etching mode, leading to InN crystal growth is prohibited. The deposition of InN is more effective by using inert carrier gas to avoid the increase of H<sub>2</sub> partial pressure.

Yang et al. (2002) proposed that the film quality can also be improved by increasing a reactant gas velocity. Besides, Yamaguchi et al. (1999) reported that the crystal quality of MOVPE grown InN thin films depends on lattice matching of substrate and film thickness, where InN film was deposited on various substrates such as GaN, AlN and sapphire, respectively. It was found that InN grown on GaN exhibits the best crystalline structure. Furthermore, it was observed that the InN film with thickness of around 400 to 1200 Å exhibits high screw dislocation, and it was dominated by grain islands with different crystalline orientations. As the film thickness exceeds 1200 Å, the residual strain was found to be gradually decreased. The improvement in the structural properties was explained to be due to the reduction in dislocation density and degree of disorientation (Lu et al., 2003a). According to Khan et al. (2008), the MOCVD grown InN epilayers exhibited the excellent electrical properties and could provide a platform for the future InN device applications. Yang et al. (2002) reported that the InN thin film with Hall mobility of 250 cm<sup>2</sup>/Vs and a carrier concentration of 1×10<sup>19</sup> cm<sup>-3</sup> at room temperature was obtained. Later, Yamamoto et al. (2006) reported that the high quality InN thin film with the highest

mobility of  $1100 \text{ cm}^2/\text{Vs}$  and lowest carrier concentration of  $4.5 \times 10^{18} \text{ cm}^{-3}$  was obtained at a relatively low V/III molar ratio.

### **2.3.2 Molecular beam epitaxy (MBE)**

MBE is an advanced process for the growth of epitaxial films. This approach is dependent upon the atomic species being deposited. To overcome the problem of atomic impurities, an ultrahigh vacuum system (around  $10^{-9}$  Torr) is required to remove the unwanted background gases, such as oxygen, which cause defects on the deposited thin films (Mukundan et al., 2015). In the vacuum ambient, a single beam or multiple beams of atoms or molecules are incident on a heated crystal substrate and produced an atomically clean surface (Arthur, 2002). For the InN crystal growth, the solid In-source is used, while the N-source is supplied by the gases such as  $\text{N}_2$  and  $\text{NH}_3$ . In the case if the metal-organic beam is applied as the element source, it is introduced as metal-organic molecular beam epitaxy (MOMBE) or chemical beam epitaxy (Abernathy et al., 1997).

Several studies reported that the  $\text{N}_2$  molecules require the high dissociation energy of about 9.5 eV, thus, the interaction of  $\text{N}_2$  gas to the substrate surface with In-source is not able to induce InN crystal growth. For obtaining reactive nitrogen atoms, RF plasma or electron cyclotron resonance (ECR) method was applied. Hughes et al. (1995) claimed that the ions generated in RF-radical source is lower than the ECR due to the high plasma pressure, and this might induce ion damage during the growth. Besides, the used of plasma system might lead to the incorporation of contamination, such as oxygen or carbon dioxide (Hoke et al., 1991). In the ECR plasma source, the generation rate of reactive nitrogen atoms can be enhanced with increasing input

microwave power. However, the nitrogen atoms with energy higher than 60 eV will induce defects in the epitaxial layer (Lee et al., 1995). Nanishi et al. (2003) reported that the MBE system equipped with an RF plasma source is advantageous in depositing high quality InN. Through this approach, neutral and ionized excited-state nitrogen atoms can be generated separately by the plasma source, while the crystal growth temperature can be controlled independently. Researchers also suggested that the generation rate of reactive nitrogen atoms can be enhanced by using aperture with small size and high density. For NH<sub>3</sub>, the source was applied to the substrate surface without dissociation. This is because the decomposition of NH<sub>3</sub> will promote the production of N<sub>2</sub> molecules (Lee et al., 1995).

A thermodynamic analysis on the MBE growth InN epilayers was reported by Koukitu and Seki (1997). Based on the phase diagram during deposition, they proposed that the suitable growth temperature is in range of 600 to 700 °C with V/III  $\geq$  1. While the thermal etching and formation of In-droplet were observed in range of 500 to 900 °C. However, the determined experimental growth temperature was found in the range of 450 to 550 °C, which is much lower than the predicted theoretically. In 2002, Davydov et al. (2002b) have successfully deposited single-crystalline hexagonal InN with a band gap value less than 1.1 eV. Saito et al. (2002) demonstrated that the highest InN crystallinity can be achieved by RF-MBE at growth temperature of 550 °C. They reported the absorption edge value of 0.75 eV was obtained in the study. Lu et al. (2003b) reported the obtained of 0.7 eV for the InN deposited on *c*-plane sapphire. In their recent study, the growth of thick InN film (up to 7.5  $\mu$ m) has led to the highest mobility of 2100 cm<sup>2</sup>/Vs with the lowest carrier concentration of  $3 \times 10^{17}$  cm<sup>-3</sup>. The structural defects or incorporation of impurities due to the unintentional doping can be reduced by depositing thicker films (Lu et al., 2011).

Chen and Kuo (2012) showed that the highly *c*-preferred orientation InN grown on gallium-doped zinc oxide (GZO) buffer was obtained by MOMBE.

### 2.3.3 Radio-frequency (RF) sputtering

RF sputtering is a widely used and the earliest successful growth technique for InN. In the sputtering process, high-kinetic energy ions are bombarded onto a source material (the target) and removed atoms from the target surface. These ejected atoms are transported in a reactive gas ambient, condense and form a thin coating on the substrate surface. Sputtering is a purely physical process, the addition of a reactive gas to the plasma is essential to deposit a compound layer (Depla et al., 2010). In the early study, Hovel and Coumo (1972) reported the success in RF sputtering growth of InN with the electron concentration of  $7 \times 10^{18} \text{ cm}^{-3}$ . In 1980s, most studies on the InN properties were reported by Tansley and Foley (1986). A prominent result was obtained, i.e. room temperature absorption edge of 1.89 eV, the highest mobility of  $2700 \text{ cm}^2/\text{Vs}$  and lowest background carrier concentration of  $5 \times 10^{16} \text{ cm}^{-3}$ . Several studies pointed out that in reactive sputtering, high growth temperature is an important factor in improving the crystallinity of InN thin film by increasing the ad-atoms energy and mobility. Braic and Zoita (2010) deduced that the InN crystal growth was improved as the substrate temperature increases from 350 to 500 °C where the hexagonal InN phase was formed. They also reported that at substrate temperature higher than 550 °C, no film was deposited due to the rapid decomposition of InN.

There is a report showed that the surface of InN can easily be oxidized when exposed to ambient air. Westra et al. (1988) showed that the high oxygen concentration of at least 11% was found in the InN film. However, the presence of

either  $\text{In}_2\text{O}_3$  or indium oxynitride ( $\text{InNO}$ ) was not observed from the crystalline structure analysis. They stated that it could be due to the formation of amorphous  $\text{InNO}$  in the  $\text{InN}$  film. The incorporation of amorphous and crystalline phases leads to the reduction in mobility and enhances the electron concentration in the deposited film. Motlan et al. (2002) reported that the  $\text{InN}$  band gap was varied with the film thickness and aging time for the film prepared by reactive sputtering. They noticed that the large absorption edge of 2.8 eV can be obtained at smaller film thickness, higher aging time and annealing temperature. The observation was described due to the formation of  $\text{InNO}$  as a result of incorporation of oxygen in the film.

Furthermore, it was reported that the reactive gas ambient plays an important role in defining the film properties by reactive sputtering. Guo et al. (1999b) studied the effects of nitrogen/argon gas ratio on the composition and structure of  $\text{InN}$  films prepared by RF magnetron sputtering. They found that the phase of the deposited films changed from indium, to indium and  $\text{InN}$ , and to  $\text{InN}$  as the  $\text{N}_2$  content in the system was increased. The wurtzite structure  $\text{InN}$  was grown in the range of 40 to 100% nitrogen content in the reactive gas, while the highly  $c$ -preferred orientation  $\text{InN}$  film was obtained in the pure nitrogen ambient. In a recent study, Amirhoseiny et al. (2011) demonstrated that the crystal quality of  $\text{InN}$  was significantly improved for the deposition in nitrogen/argon mixture ambient.  $\text{InN}$  films with greater crystallite size were obtained for the deposition in 50:50 (nitrogen:argon) gas ratio than those deposited in pure nitrogen ambient. In addition, they observed that the film thickness was enhanced with increasing argon content in the deposition ambient due to the higher electron capture ability of nitrogen than argon which decreases the density of plasma. They claimed that the higher density of plasma is able to eject more indium-

atoms from the target surface and react with  $N_2$  to form InN coating on the substrate. Thus, greater InN film thickness was achieved.

### **2.3.4 Hydride vapor phase epitaxy (HVPE)**

HVPE has received intense attention due to its high growth rate compared to the MOCVD and MBE, which make it the excellent choice for the growth of thick film (Hemmingsson et al., 2010). HVPE is a chemical vapor deposition technique which carry out in a hot wall reactor (horizontal or vertical) at atmospheric pressure. For the synthesis of InN, the common source materials such as indium trichloride ( $InCl_3$ ) and  $NH_3$  gas are commonly used as the In-source and N-source, respectively.

The first InN epitaxial growth using this approach was presented by Marasina et al. (1977). They reported on the relation between the evaporation of  $InCl_3$  and epilayer growth of InN. It was found that the optimum evaporation temperature of  $InCl_3$  is in range of 450 to 520 °C. The increase of evaporation temperature from 450 to 600 °C along with the increase in  $InCl_3$  concentration has resulted in higher growth rate at the constant substrate temperature of 630 °C. Sato and Sato (1994) showed that the InN film was obtained using indium chloride ( $InCl$ ) and  $NH_3$  gas over the growth temperature ranging from 455 to 510 °C. They also reported that the electrical characteristics of the film were degraded with reducing  $NH_3$  gas flow rate. Kumagai et al. (2001) reported that the growth of InN through the chemical reaction between  $InCl$  and  $NH_3$  gas was restricted. They found that the equilibrium partial pressure and driving force in the reaction were low due to the increase in  $H_2$  molar ratio. On the contrary, Sunakawa et al. (1996) proposed that the interaction between  $InCl_3$  and  $NH_3$  gas has promoted the InN crystal growth under a condition with inert carrier gas. The

application of N<sub>2</sub> as the carrier gas was essential to promote the growth of InN, while the use of H<sub>2</sub> carrier gas has prohibited the formation of InN. Takahashi et al. (1997) demonstrated that the InN epilayer was reproducibly at the high growth temperature of 750 °C. They deduced that a high input partial pressure of InCl<sub>3</sub> was required to induce the growth of InN at the relatively high temperatures.

### 2.3.5 Other Growth Methods

Other methods used to synthesis InN thin films include pulsed laser deposition (PLD), reactive evaporation and solvo-thermal. The PLD technique is a vacuum based process which can produce high quality III-nitride films at lower growth temperature. A thin coating is deposited on the substrate surface by laser ablation of a target (An et al., 2003). The first attempt to synthesize InN film on sapphire(0001) substrate using PLD was carried out by Feiler et al. (1997). Here, InN film was formed in N<sub>2</sub> ambient under high vacuum condition. Although they reported that the deposited film was not in single crystal, it exhibited *p*-type conductivity with a carrier concentration of  $6.2 \times 10^{20} \text{ cm}^{-3}$  and a mobility of 240 cm<sup>2</sup>/Vs. However, the formation of In-droplets was found on the film surface. Fernández et al. (2000) suggested that good quality InN film can be produced by providing reactive N<sub>2</sub> through a low-energy atomic beam. This approach is able to avoid the incorporation of hydrogen source during deposition and reduce the dependence on substrate temperature to overcome the kinetic barrier for InN crystal growth. There is a report by Bhattacharya et al. (2002) demonstrating InN crystal growth at 400 °C through N<sub>2</sub> glow discharge plasma-assisted PLD using In-target. They showed that the InN optical band gap of 1.9 eV was obtained.

Among the aforementioned methods, reactive evaporation is the simplest and most reported growth method. A thin coating is deposited on a substrate surface by evaporating a metal source in a chamber in the presence of reactive gas. Trainor and Rose (1974) reported the successful growth of InN film on sapphire and showed that InN is a direct band gap semiconductor with a band edge energy of 1.7 eV. Besides, they suggested that the thermal annealing under a high atomic nitrogen pressure condition is essential to form stoichiometric layer. According to Sato and Sato (1995), the reduction of growth rate has effectively lowered the carrier concentration of the InN film from about  $10^{20}$  to  $10^{18}$   $\text{cm}^{-3}$ . Solvo-thermal is a recent reported deposition technique where Bai et al. (2002) demonstrated that InN nanocrystals with an average size of 28 nm can be obtained by the reaction of  $\text{InCl}_3$  and lithium nitride ( $\text{Li}_3\text{N}$ ) with xylene solvent at 250 °C. Recently, Barick and Dhar (2015) showed that InN nanocrystals can be prepared through nitridation of lithium-indium oxide ( $\text{LiInO}_2$ ) with sodium amide ( $\text{NaNH}_2$ ) at 170 to 240 °C. It was found that the wurtzite InN crystals with an average size of 100 nm were formed at a low nitridation temperature of 170 °C. In addition, they pointed out that the carrier concentration and density defect in the InN crystals were increased with decreasing growth temperatures. The various deposition approaches and outcomes are summarized in Appendix A.

## **2.4 An overview on sol-gel spin coating method**

Sol-gel process allows the formation of solid materials through gelation of solution. ‘Sol’ is defined as a stable suspension of solid particles in a solvent, a network structure, namely, ‘gel’ is formed when interaction between discrete particles in the sol becomes extensive (Danks et al., 2016). According to Brinker and Scherer